

# Search for Heavy Neutral Leptons with IceCube DeepCore

## **Dissertation**

zur Erlangung des akademischen Grades  
doctor rerum naturalium  
(Dr. rer. nat.)

im Fach: Physik  
Spezialisierung: Experimentalphysik

eingereicht an der  
Mathematisch-Naturwissenschaftlichen Fakultät  
der Humboldt-Universität zu Berlin

von

**Leander Fischer M. Sc.**  
geboren am 24. Oktober 1992  
in Heidelberg

Präsidentin der Humboldt-Universität zu Berlin  
Prof. Dr. Julia von Blumenthal

Dekanin der Mathematisch-Naturwissenschaftlichen Fakultät  
Prof. Dr. Caren Tischendorf

**Copyright Notice**

This book is released into the public domain using the CC-BY-4.0 code.

To view a copy of the CC-BY-4.0 code, visit:

<https://creativecommons.org/licenses/by/4.0/>

**Colophon**

This document was typeset with the help of KOMA-Script and L<sup>A</sup>T<sub>E</sub>X using the open-source kaobook template class.

The source code of this thesis is available at:

[https://github.com/LeanderFischer/phd\\_thesis](https://github.com/LeanderFischer/phd_thesis)

# Todo list

add fancy icecube picture . . . . .	1
exchange for figure with scattering (check abs/sca is cocorrect) . . . . .	2
mention/cite dust logger paper/procedure? . . . . .	2
Maybe throw the coordinate system in a box on the side? . . . . .	3
Add reference for these processes. . . . .	6
cite em shower distribution . . . . .	6
add angular profile plot? (create one based on leif Radel as alex did) . . . . .	6
increase main text width (read in kao docu) . . . . .	9
put a number on this significant increase? . . . . .	13
put a number on the tilt angle? . . . . .	14
add plot with ice scattering/absorption lengths used for simulation . . . . .	14
add table with typical vuvuzela noise parameters . . . . .	15
add figure with trigger efficiencies (SMT 3,4,6,8) . . . . .	16
add example plots (2?) for L3 cut variables and applied cuts . . . . .	17
reference BDT . . . . .	17
add figure with L4 BDT classifier outputs . . . . .	18
add some figure showing the corridors? . . . . .	18
add table with rater per level (split in flavor for signal (benchmark mass/mixing?) and background) . . . . .	18
add image with selected strings used for flernn IC and DC . . . . .	19
add FLERCNN architecture image? . . . . .	19
add some performance plots of the FLERCNN reconstruction . . . . .	19
There is more information on pre-processing the samples and preparing the input features, and training each cnn, but I'm not sure if that might be too much detail? . . . . .	19
add table with final analysis cuts . . . . .	20
there is some more information in Elis as thesis about the final sample composition . . . . .	20
at some place I will want a selection efficiency for SM BG and HNL signal, but I'm not sure where to put it yet . . . . .	20
which experiments measure the axial mass? . . . . .	20
add varied total cross-section for a few background HNL events . . . . .	20
add final level effects of varying the axial mass parameters (or example of one) . . . . .	20
add DIS systematic effect on final level histograms . . . . .	20
add muon systematic effects (total scale and ) on final level histograms . . . . .	21



# Contents

<b>Contents</b>	<b>v</b>
<b>1 The IceCube Neutrino Observatory</b>	<b>1</b>
1.1 Detector Components . . . . .	1
1.1.1 Digital Optical Modules and the Antarctic Ice . . . . .	2
1.1.2 IceCube . . . . .	3
1.1.3 DeepCore . . . . .	3
1.2 Particles Propagation in Ice . . . . .	4
1.2.1 Cherenkov Effect . . . . .	4
1.2.2 Energy Losses . . . . .	5
1.3 Event Morphologies . . . . .	7
<b>2 Standard Model Background Simulation and Data Processing</b>	<b>11</b>
2.1 Event Generation . . . . .	11
2.1.1 Neutrinos . . . . .	12
2.1.2 Muons . . . . .	13
2.2 Detector Simulation . . . . .	13
2.2.1 Photon Propagation . . . . .	14
2.2.2 Detector Responses . . . . .	14
2.3 Processing . . . . .	15
2.3.1 Trigger and Filter . . . . .	15
2.3.2 Event Selection . . . . .	16
2.4 Reconstruction . . . . .	18
2.4.1 Fast Low Energy Reconstruction using Convolutional Neural Networks . . . . .	18
2.4.2 Analysis Selection . . . . .	19
2.5 Systematic Uncertainties . . . . .	20
2.5.1 Atmospheric Flux . . . . .	21
2.5.2 Detector Property Variations . . . . .	21
<b>Bibliography</b>	<b>23</b>



# List of Figures

1.1	IceCube overview . . . . .	1
1.2	IceCube sideview . . . . .	2
1.3	Digital Optical Module (DOM) . . . . .	3
1.4	IceCube top view . . . . .	4
1.5	Cherenkov light front . . . . .	5





# List of Tables

1.1	IceCube event signatures and underlying interactions . . . . .	8
2.1	GENIE generation cylinder volumes . . . . .	13



# The IceCube Neutrino Observatory

# 1

The IceCube Neutrino Observatory [1] is a cubic-kilometer, ice-Cherenkov detector located at the geographic South Pole. IceCube utilizes the Antarctic glacial ice as detector medium to observe neutrinos by measuring the Cherenkov light produced from secondary charged particles with optical modules. It was deployed between 2006 and 2011 and has been taking data since the installation of the first modules. The primary goal of IceCube is the observation of astrophysical neutrinos as a telescope, but it can also be used to study fundamental particle physics properties by measuring atmospheric neutrinos as well as studying cosmic rays.

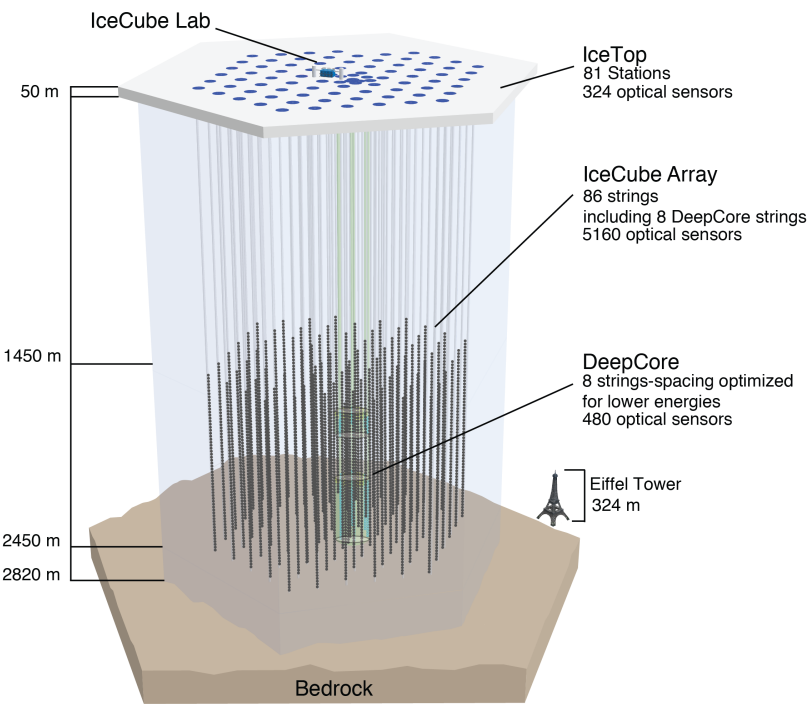
This chapter first describes the main- and sub-array of the detector and its detection module in Section 1.1, the propagation of particles through ice is explained in Section 1.2, and finally, the signatures that IceCube can observe of the different particles are introduced in Section 1.3.

add fancy icecube picture

1.1	Detector Components . . .	1
1.2	Particles Propagation in Ice . . . . .	4
1.3	Event Morphologies . . . .	7

[1]: Aartsen et al. (2017), “The IceCube Neutrino Observatory: instrumentation and online systems”

## 1.1 Detector Components



**Figure 1.1:** Overview of the IceCube detector showing the in-ice main- and sub-array IceCube and DeepCore, IceTop, and the IceCube Lab. From [1].

The full IceCube detector array consists of 86 vertical, in-ice strings and 81 surface stations as shown in Figure 1.1. The in-ice part is composed of 60 optical modules per string deployed at depths of 1450 m–2450 m below the ice, while the surface stations of the comic air-shower array, *IceTop*, are ice-filled tanks. The surface stations and the majority of the strings are arranged in a hexagonal grid with the operations building, the *IceCube Laboratory* (ICL), central to the grid on the surface. A top view

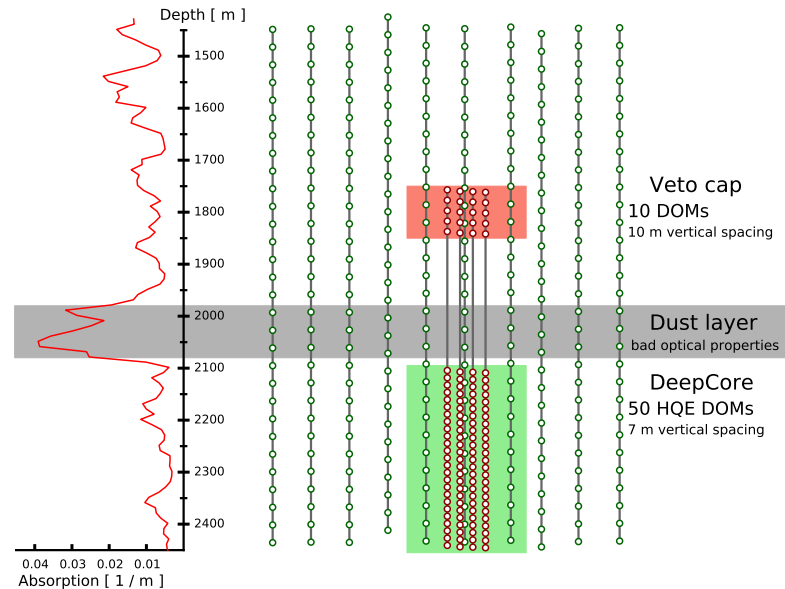
of the hexagonal arrangement is shown in Figure 1.4. The in-ice array is designed to detect neutrinos in the energy range from GeV to PeV.

### 1.1.1 Digital Optical Modules and the Antarctic Ice

The IceCube detection medium is the Antarctic glacial ice itself, which was formed over 100 000 years by accumulation of snow that was subsequently compressed by its own weight to form a dense crystal structure [2]. As a result of this formation process, the optical properties, scattering and absorption, primarily change with depth. Within the detector volume the absorption length ranges from 100 m–400 m, while the scattering length lies between 20 m and 100 m. They are correlated, with the absorption length being roughly four times the scattering length [3]. The vertical distribution of scattering and absorption length can be seen in Figure 1.2, where one dominant feature is the *dust layer* between 2000 m and 2100 m depth. This region has a higher concentration of dust particles that were deposited in a period of high volcanic activity, which leads to bad optical properties in form of larger scattering and absorption.

[2]: Price et al. (2000), “Age vs depth of glacial ice at South Pole”

[3]: Abbasi et al. (2022), “In-situ estimation of ice crystal properties at the South Pole using LED calibration data from the IceCube Neutrino Observatory”



**Figure 1.2:** Side view of IceCube and DeepCore showing the depth dependent scattering and absorption length (left panel) and the DOM positions around the dust layer.

exchange for figure with scattering (check abs/sca is correct)

mention/cite dust logger paper/procedure?

[4]: Abbasi et al. (2009), “The IceCube data acquisition system: Signal capture, digitization, and timestamping”

[4]: Abbasi et al. (2009), “The IceCube data acquisition system: Signal capture, digitization, and timestamping”

The ice is instrumented by 5160 optical sensors called *Digital Optical Modules* (DOMs) [4], which can detect the Cherenkov light produced by charged particles traveling through the ice. Each DOM is made of a spherical glass housing, containing a downward-facing Photomultiplier Tube (PMT), the main-board with control, readout, and processing-electronics, and a LED flasher-board for calibration purposes. The design and the individual components of a DOM can be seen in Figure 1.3.

The majority of PMTs are the 10” Hamamatsu R7081-02, which have a bialkali photocathode and are sensitive to wavelengths in the range of 300 nm to 650 nm, with a peak quantum efficiency of 25% at 390 nm. In the central part of the IceCube array the peak efficiency reaches 34%. The dark count rate in the temperature range of  $-40^{\circ}\text{C}$  to  $-20^{\circ}\text{C}$  is  $\sim 300$  Hz. The DOM electronics measure the PMT voltage and control the gain. At a voltage crossing of the equivalent to 0.25 PE the waveform readout is activated [4]. Only when either one of the nearest or next to nearest

DOMs above or below also saw a voltage crossing within a  $1\ \mu\text{s}$  time window<sup>1</sup>, the voltages are digitized and send to the ICL. Through the application of a waveform unfolding algorithm, called *WaveDeform* [5], the waveforms are compressed and the results are the reconstructed times and charges of the photo-electrons. This is the basis for all further IceCube data processing.

The PMT is covered with a mu-metal grid (made from wire mesh), shielding the photocathode from Earth's magnetic field and it is optically coupled to the glass sphere by RTV silicone gel. The glass sphere is a pressure vessel, designed to withstand both the constant ice pressure and the temporary pressure during the refreezing process of the water in the drill hole during deployment (peaking at around 690 bar). The sphere is held by a harness that connects the DOMs along a string and also guides the cable beside them.

The flasher-board controls 12 LEDs that produce optical pulses in bright UV. The LEDs can be pulsed separately or in combination with variable output levels and pulse lengths. Using the known information of the light source positions and times this can be used for in-situ calibration of the detector by measuring absorption and scattering properties of the ice. Calibrating the optical efficiency of the DOMs itself is more accurately done using minimum ionizing muons [6], since the total amplitude of the LED light is not well known.

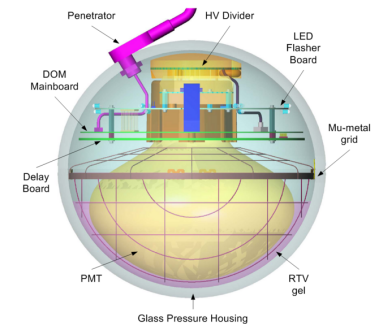
### 1.1.2 IceCube

The 78 strings that are arranged in a hexagonal pattern from the main part of the in-ice array, which is called *IceCube*. With a  $\sim 125\ \text{m}$  horizontal spacing between the strings and a  $\sim 17\ \text{m}$  vertical spacing between DOMs, IceCube has a lower energy threshold of around 100 GeV. IceCube was designed to detect astrophysical neutrinos with energies above 1 TeV.

The coordinate system that is used in IceCube is centered at 46500'E, 52200'N at an elevation of 883.9 m [1]. Per definition, it's a right-handed coordinate system where the y-axis points along the Prime Meridian (Grid North) towards Greenwich, UK, and the x-axis points 90° clockwise from the y-axis (Grid East). The z-axis is normal to the ice surface, pointing upwards. For IceCube analyses depth is defined as the distance along the z axis from the ice surface, assumed to be at an elevation of 2832 m.

1: This is referred to as a *hard local coincidence (HLC)* [4].

[5]: Aartsen et al. (2014), "Energy Reconstruction Methods in the IceCube Neutrino Telescope"



**Figure 1.3:** Design and components of a Digital Optical Module (DOM) [4]

[6]: Kulacz (2019), "In Situ Measurement of the IceCube DOM Efficiency Factor Using Atmospheric Minimum Ionizing Muons"

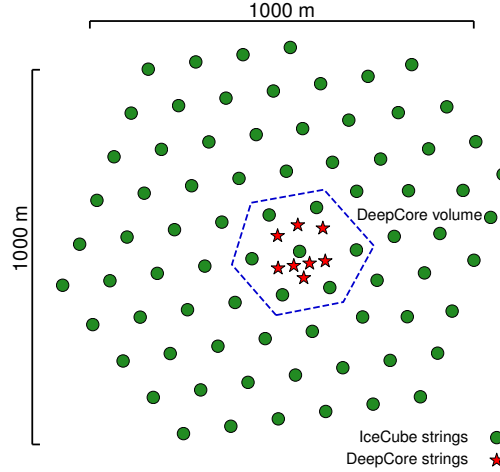
[1]: Aartsen et al. (2017), "The IceCube Neutrino Observatory: instrumentation and online systems"

Maybe throw the coordinate system in a box on the side?

### 1.1.3 DeepCore

The additional 8 strings form a denser sub-array of IceCube called *DeepCore* [7]. It's located at the bottom-center of the in-ice array and its *fiducial volume* also includes the 7 surrounding IceCube strings as shown in Figure 1.4. The strings in this region have a closer average horizontal distance of about 70 m. The lower 50 DeepCore DOMs on each string are placed in the region of clear ice below the dust layer between 2100 m to 2450 m depth, where their vertical spacing is  $\sim 7\ \text{m}$ . The remaining 10 modules on each string are placed above the dust layer to be used as veto against atmospheric muons as can be seen in Figure 1.2. Additionally, the

[7]: Abbasi et al. (2012), "The design and performance of IceCube DeepCore"



**Figure 1.4:** Top view of the IceCube array.

DeepCore DOMs are equipped with higher quantum efficiency PMTs. The combination of the denser spacing and the high quantum efficiency modules, leads to a lower energy detection threshold of around 5 GeV, allowing the observation of atmospheric neutrinos, which are mostly in the energy range of 10 GeV to 100 GeV. The main analysis performed with DeepCore is an atmospheric neutrino oscillation measurement, but the large flux of atmospheric neutrinos allows for many other Beyond Standard Model searches, such as searches for dark matter, non-standard interactions, or sterile neutrinos.

## 1.2 Particles Propagation in Ice

Neutrinos interacting in the ice via DIS produce muons, electromagnetic showers, and hadronic showers, depending on their flavor and the interaction type. The particles produced in those processes mainly lose their energy through *ionization*, *bremsstrahlung*, *pair production*, and the *photo-nuclear interaction*. Electrically charged particles also emit Cherenkov light when traveling through the ice, which is the main observable in IceCube, but only contributes a small amount to the total energy loss. The Cherenkov effect and the energy losses of the particles are described in the following sections, followed by an overview of the different particle signatures in IceCube.

### 1.2.1 Cherenkov Effect

When a charged particle moves through a medium with a velocity that is greater than the speed of light in that medium, it emits Cherenkov radiation, losing a very small amount of energy ( $\mathcal{O}(10^{-4})$  of the total energy loss). The detection principle of IceCube and DeepCore however, is based fundamentally on the observation of resulting Cherenkov photons that are emitted by the charged secondary particles produced in the neutrino interactions that were introduced in Section ???. The Cherenkov effect was first observed by Pavel Cherenkov in 1934 [8] and occurs when the charged particle travels faster than the phase velocity of light, therefore polarizing the medium. Upon de-excitation the molecules emit the received energy

[8]: Cherenkov (1937), “Visible Radiation Produced by Electrons Moving in a Medium with Velocities Exceeding that of Light”

as photons in a spherical wavefront. Since the particle moves past this wavefront, the superposition of the spherical light emissions form a cone which is shown in blue in the bottom of Figure 1.5.

Using trigonometry, the angle  $\theta_c$  at which the Cherenkov light is emitted can be calculated as

$$\theta_c = \arccos\left(\frac{1}{\beta n}\right), \quad (1.1)$$

where  $\beta$  is the velocity of the particle in units of the speed of light and  $n$  is the refractive index of the medium. When the particle velocity is close to the speed of light, the equation holds and the angle is only dependent on the refractive index of the medium. For the Antarctic ice, the refractive index is  $n \approx 1.3$  and as a result  $\theta_c \approx 41^\circ$  [9].

The frequency of the emission depends on the charge  $z$  and the wavelength-dependent index of refraction  $n(\omega)$  and is given by the Frank-Tamm formula [10, 11]

$$\frac{d^2N}{dx d\lambda} = \frac{2\pi\alpha z^2}{\lambda^2} \left(1 - \frac{1}{\beta^2 n(\omega)^2}\right), \quad (1.2)$$

with  $\alpha \approx 1/137$  the fine structure constant,  $\lambda$  the wavelength of the emitted light, and  $x$  the path length traversed by the particle. Relativistic particles in ice produce roughly 250 photons per cm in the wavelength range of 300 nm-500 nm [12].

### 1.2.2 Energy Losses

Even though relativistic, charged particles traveling through matter produce Cherenkov radiation, their energy is mainly lost through other processes that are dependent on the particle type and energy. The exact principles of energy loss for the different types can broadly be categorized into the three groups: quasi-continuous energy loss by muons, electromagnetic cascades, and hadronic cascades.

#### Muons

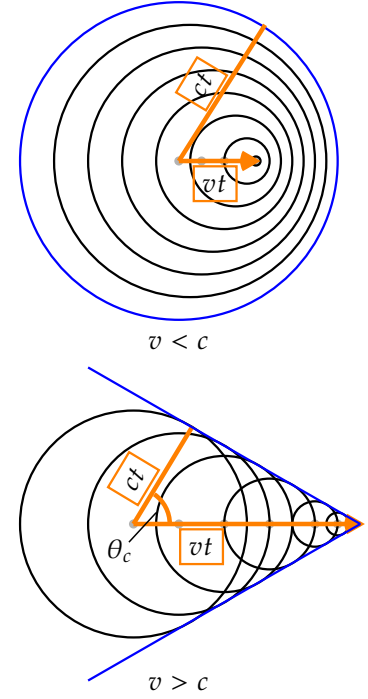
Muons lose their energy by ionization, bremsstrahlung, pair production, and the photo-nuclear effect. The energy loss by ionization is the dominant process for muons above 1 GeV and has a weak energy dependence given by

$$\left\langle -\frac{dE}{dx} \right\rangle = a_I(E) + b_R(E) \cdot E, \quad (1.3)$$

where  $E$  is the energy and  $a_I(E)$  and  $b_R(E) \cdot E$  are the energy loss by ionization and the combined radiative losses, respectively. In the energy range relevant for this work (10 GeV-100 GeV), the parameters  $a_I$  and  $b_R$  only depend on energy very weakly and can be approximated by constants. The energy loss is then given by

$$\left\langle -\frac{dE}{dx} \right\rangle = a + b \cdot E. \quad (1.4)$$

Based on this description, there is a critical energy which divides the regimes where ionization and radiative losses dominate. The critical



**Figure 1.5:** Schematic depiction of the spherical light front produced by a particle traveling slower than the speed of light in the medium (top) and the formation of the Cherenkov light front produced by a charged particle traveling faster than the speed of light in the medium (bottom). Blue is the resulting wavefront, while the black circles are spherically emitted light at each position and the orange arrows show the direction of the particle.

[9]: Euler (2014), "Observation of oscillations of atmospheric neutrinos with the IceCube Neutrino Observatory"

[10]: Frank et al. (1937), "Coherent visible radiation from fast electrons passing through matter"

[11]: Tamm (1991), "Radiation Emitted by Uniformly Moving Electrons"

[12]: Rädcl et al. (2012), "Calculation of the Cherenkov light yield from low energetic secondary particles accompanying high-energy muons in ice and water with Geant4 simulations"

[13]: Chirkin et al. (2004), “Propagating leptons through matter with Muon Monte Carlo (MMC)”

energy is given by  $E_{crit} = a/b$  and for muons in ice it is  $\sim 713$  GeV (using  $a \approx 2.59$  MeV and  $b \approx 3.63 \times 10^{-6} \text{ cm}^{-1}$  [13]). Since the energy range of interest is well below this critical energy the range of a muon can easily related to its energy by

$$\langle L \rangle = \frac{E_0}{a} , \quad (1.5)$$

Measuring the length of a muon track therefore allows for an estimation of its energy if the full track is contained in IceCube. Using the given numbers a 30 GeV muon travels  $\sim 116$  m. This approximate treatment does not take into account the stochastic nature of some energy losses. Bremsstrahlung and photo-nuclear interactions for example occur rarely, but when they do, they deposit a large chunk of energy. A thorough investigation of the energy losses of muons in ice can be found in [14].

[14]: Raedel (2012), “Simulation Studies of the Cherenkov Light Yield from Relativistic Particles in High-Energy Neutrino Telescopes with Geant4”

### Electromagnetic Showers

Photons as well as electrons and positrons are produced either directly in neutrino interactions or in secondary particle interactions. Above a critical energy  $E_c$ , they lose their energy through pair production and bremsstrahlung, respectively, where the resulting photons and the electron/positron pairs can both produce further particles through repeated pair production and bremsstrahlung emission forming an expanding, electromagnetic shower profile. The particles’ energy reduces with every interaction and their number increases until they fall below the critical energy where ionization and excitation of surrounding atoms become the dominant energy loss processes for electrons and positrons. For photons the remaining energy is lost through the Compton effect and the photoelectric effect. Below the critical energy no new shower particles are produced. Electromagnetic cascades can be characterized by the radiation length,  $X_0$ , after which electrons/positrons reduced their energy to  $1/e$  of their initial energy. For photons, it’s equivalent to  $7/9$  of the mean free path of pair production. The critical energy for ice is  $E_c \approx 78$  MeV, with a radiation length of  $X_0 \approx 39.3$  cm [15].

Add reference for these processes.

[15]: Tanabashi et al. (2018), “Review of Particle Physics”

cite em shower distribution

The radiation length governs the longitudinal shower profile and using  $t = x/X_0$ , the shower intensity can be described by

$$\frac{dE}{dt} = E_0 b \frac{(bt)^{a-1} e^{-bt}}{\Gamma(a)} , \quad (1.6)$$

[14]: Raedel (2012), “Simulation Studies of the Cherenkov Light Yield from Relativistic Particles in High-Energy Neutrino Telescopes with Geant4”

[16]: Agostinelli et al. (2003), “Geant4—a simulation toolkit”

where  $a$  and  $b$  are parameters that have to be estimated from experiment. Based on the work from [14], performed with Geant4 [16], the parameters for electromagnetic showers in ice are

$$e^- : a \approx 2.01 + 1.45 \log_{10}(E_0/\text{GeV}), b \approx 0.63 , \quad (1.7a)$$

$$e^+ : a \approx 2.00 + 1.46 \log_{10}(E_0/\text{GeV}), b \approx 0.63 , \quad (1.7b)$$

$$\gamma : a \approx 2.84 + 1.34 \log_{10}(E_0/\text{GeV}), b \approx 0.65 . \quad (1.7c)$$

The maximum of the shower is at  $t_{max} = (a - 1)/b$  and the Cherenkov emission of the charged particles produced in the shower is peaked around the Cherenkov angle, since they are produced in the forward direction.

add angular profile plot?  
(create one based on leif R  del as alex did)



## Hadronic Showers

The breaking nucleus or any hadronic decay products from the neutrino DIS interactions always create a hadronic cascade. It is a result of secondary particles produced in strong interactions between the hadrons and the traversed matter. The charged particles produced in the shower will emit Cherenkov radiation, while neutral particles will be invisible to the detector. There is also an electromagnetic component of the shower, due to for example the decay of neutral pions into photons. Hadronic showers of the same energy as electromagnetic showers have larger fluctuations in energy deposition and shape, since they depend on the produced particle types. Hadrons also have a higher energy threshold for Cherenkov light production, because of their higher mass. Based on [14, 17], the visible electromagnetic fraction of hadronic showers can be parameterized as

$$F(E_0) = \frac{T_{\text{hadron}}}{T_{\text{EM}}} = 1 - (1 - f_0) \left( \frac{E_0}{E_s} \right)^{-m}, \quad (1.8)$$

where  $T_{\text{hadron/EM}}$  is the total track length of a hadronic/electromagnetic shower with the same energy,  $f_0$  is the ratio of hadronic and electromagnetic light yield,  $E_0$  is the initial energy, and  $E_s$  is an energy scale. The parameter  $m$  is an arbitrary parameter. The ration  $F(E_0)$  increases with energy, but is always smaller than 1. The variance of this distribution is given by

$$\sigma_F(E_0) = \sigma_0 \log(E_0)^{-\gamma}. \quad (1.9)$$

The parameters  $m$ ,  $E_s$ , and  $f_0$  are fit from simulation. Cherenkov light from hadronic showers also peaks around the Cherenkov angle, but the angular distribution is more smeared out, due to the variations in particle type and their energy depositions.

[14]: Raedel (2012), “Simulation Studies of the Cherenkov Light Yield from Relativistic Particles in High-Energy Neutrino Telescopes with Geant4”

[17]: Gabriel et al. (1994), “Energy dependence of hadronic activity”

## 1.3 Event Morphologies


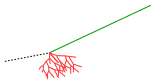

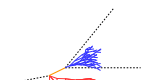
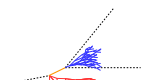

The event morphologies produced by particles detected in IceCube are combinations of the three energy loss types described in Section 1.2.2, e.g. *cascades* from electromagnetic and hadronic showers and elongated *tracks* from muons traveling through the detector. Table 1.1 gives an overview of the possible event signatures.

**Neutrino** interactions are observed as cascades, tracks, or a combination of both, depending on the initial flavor and the interaction type for the specific event.

In  $\nu_\mu$  - CC interactions, a muon is produced in addition to a hadronic shower from the breaking nucleus. If the interaction happens outside the detector, but the muon passes through the detector, this will create a track-like signature. Same happens if the interaction happens inside, but the energy transfer to the nucleus is small ( $y \approx 0$ ). At energies relevant for this work, tracks have length at the same order of the distance between DOMs, so they can be observed as such.

If the interaction happens inside the detector and the energy transfer to the hadronic part of the shower is larger, it will create a cascade with

**Table 1.1:** IceCube event signatures, their underlying interaction type, and the particles that produce them. Also shown are the secondary particles produced in the interactions. Black dashed lines represent neutrinos, green lines muons, orange line leptons, and blue and red lines are particles in electromagnetic and hadronic cascades, respectively. Adapted from [18].

Interaction	Secondary particles	Signature
$\text{CC } \nu_\mu^{(-)}$	 $\mu^\pm$ track	Track-only
	 $\mu^\pm$ track and hadrons	Track with cascade
$\text{CC } \nu_\tau^{(-)}$	 $\tau^\pm$ decaying into $\mu^\pm$ ( $\sim 17\%$ BR), hadrons	Cascade with track
	 $\tau^\pm$ decaying into $e^\pm$ or hadrons ( $\sim 83\%$ BR)	
$\text{CC } \nu_e^{(-)}$	 $e^\pm$ , hadrons	Cascade-only
$\text{NC } \nu_\ell^{(-)}$	 hadrons	

a track leaving it. A similar signature occurs if a  $\nu_\tau$  - CC interaction happens, creating a tau that decays into a muon (happening with a branching ratio of 17%). In those cases the muon usually has a lower energy and the track will be fainter and harder to observe.

The other 83 % of  $\nu_\tau$  - CC interactions produce a tau that decays into an electron or hadrons, leaving a cascade-only signature through the electromagnetic or hadronic shower. All  $\nu_e$  - CC interactions also produce pure cascades, since the electron quickly loses its energy in an electromagnetic shower. In all  $\nu$  - NC interactions, the produced neutrino escapes and only the hadronic shower is observable. Since the size of the cascades at the energy range of interest is smaller than the spacing of the DOMs, they are approximately observed as point-like, spherical light sources. Considering the short effective scattering length (20 m-50 m), the light is almost isotopically emitted.

**Atmospheric muons** also produce pure track like signatures, similar to  $\nu_\mu$  - CC interactions happening outside the detector. They are one of the main backgrounds for analyses using atmospheric neutrinos and are therefore the target of many filter steps described in Section 2.3.1.

increase main text width  
(read in kao docu)



# Standard Model Background Simulation and Data Processing

# 2

The analysis presented in this thesis is highly dependent on an efficient event selection to reduce the raw IceCube trigger data to a usable atmospheric neutrino sample. Based on this selection a precise estimation of both expected SM background and expected BSM signal events can be made using MC simulations. This chapter describes the current simulation and event selection chain used for state-of-the-art IceCube neutrino oscillation measurements like [19]. The whole chain can be broadly split into 4 steps:

**Step 1 Event Generation:** The initial step for all particle (non-noise) simulation is the generation of events from selected initial distributions and fluxes. Events are the primary particle and the particles produced in the interaction with the ice.

**Step 2 Detector Simulation:** The particles from the first step are propagated through the ice, producing Cherenkov photons, which are then propagated further until they reach a DOM or are absorbed. If they hit a DOM the detector response (acceptance and PMT) is simulated.

**Step 3 Processing:** Starting from the PMT output, both real data and simulation are processed through the in-ice trigger, the online filter and processing, and the low energy event selection to produce a neutrino dominated sample.

**Step 4 Reconstruction:** Once the sample is small enough for more sophisticated reconstruction techniques to be feasible to run, the events are reconstructed using a CNN and some high level variables are computed. Based on these variables the final event selection is applied.

This chapter only describes the event generation for the SM background simulation (neutrinos and muons), while the signal simulation is described in Chapter ???. The detector simulation is identical for both signal and background events while processing and reconstruction are applied to all simulation and data in the same way. Splitting the simulation steps has the advantage of reusing the outputs of for example the generation step to propagate the particles with different ice model, in order to estimate the systematic impacts of uncertainties of the ice properties. Similar approach can be taken for varying detector response and through this a more efficient (reduced) use of computing resources can be achieved. The following sections describe the different steps in more detail and the last section, Section 2.5, describes the related systematic uncertainties considered for this work.

2.1	Event Generation . . . . .	11
2.2	Detector Simulation . . . . .	13
2.3	Processing . . . . .	15
2.4	Reconstruction . . . . .	18
2.5	Systematic Uncertainties . . . . .	20

[19]: Abbasi et al. (2023), “Measurement of atmospheric neutrino mixing with improved IceCube DeepCore calibration and data processing”

## 2.1 Event Generation

The MC is used in the analysis by applying a method called *forward folding*, where a very large number of events (signal and background) is produced using sampling distribution that are tuned to have a large selection efficiency. Those distributions don’t have to be physically correct

distributions, but they need to cover the full parameter space of interest for the analysis. To produce the correct physical distributions each event gets a weight, which can be used to estimate the expected number of events given a specific choice of physics and nuisance parameters. The large number of raw MC events ensures a good estimation of the expected numbers and weighted distributions.

The analysis itself is then performed by comparing the weighted MC distributions to the observed data. This is done by binning them as will be described in Chapter ?? and calculating a loss function comparing the bin expectations to the data. By varying the physics and nuisance parameters, that govern the weights, the loss function can be minimized and the parameters producing MC that describes the data best are found. In order to achieve a reliable result with this method the MC needs to be precise and as close to the data as possible (at least at the final selection step).

### 2.1.1 Neutrinos

Due to the very low interaction rate of neutrinos, the event generation is performed in a way that forces every event to interact in a chosen sampling volume. The weight of each event is then calculated as the inverse of the simulated neutrino fluence

$$w = \frac{1}{F_{\text{sim}}} \frac{1}{N_{\text{sim}}} , \quad (2.1)$$

where  $F_{\text{sim}}$  is the number of neutrino events per energy, time, area, and solid angle and  $N_{\text{sim}}$  is the number of simulated events. If this weight is multiplied by the livetime and the theoretically expected neutrino flux for a given physical model, it results in the number of events that this event would produce. The used baseline neutrino flux computed for the South Pole is taken from [20].

[20]: Honda et al. (2015), “Atmospheric neutrino flux calculation using the NRLMSISE-00 atmospheric model”

The chosen simulation volume is a cylinder centered in DeepCore with radius and height chosen such that all events possibly producing a signal are contained. The different sizes are chosen depending on energy and neutrino flavor are shown in Table 2.1. The directions of the neutrinos are sampled isotropically in zenith and azimuth and the energies are sampled from a power law  $E^{-2}$ . The number of simulated events is chosen such that the livetime is more than 70 years for each flavor. Neutrinos and antineutrinos are simulated with ratios of 70% and 30%, respectively.

[21]: Andreopoulos et al. (2015), “The GENIE Neutrino Monte Carlo Generator: Physics and User Manual”

[22]: Koehne et al. (2013), “PROPOSAL: A tool for propagation of charged leptons”

[16]: Agostinelli et al. (2003), “Geant4—a simulation toolkit”

[12]: Rädcl et al. (2012), “Calculation of the Cherenkov light yield from low energetic secondary particles accompanying high-energy muons in ice and water with Geant4 simulations”

To simulate the neutrino interaction with the ice the GENIE event generator [21] is used resulting in the secondary particles and the kinematic and cross-section parameters. Muons produced in these interactions are propagated using PROPOSAL [22], also simulating their Cherenkov light output. The shower development of gamma rays, electrons, and positrons below 100 MeV and hadronic showers below 30 GeV is simulated using GEANT4 [16] while for higher energies an analytical approximation from [12] is used.

Flavor	Energy [GeV]	Radius [m]	Length [m]	Events/File	Files
$\nu_e + \bar{\nu}_e$	1-4	250	500	450000	650
	4-12			100000	
	12-100	350	600	57500	
	100-10000	550	1000	6700	
$\nu_\mu + \bar{\nu}_\mu$	1-5	250	500	408000	1550
	5-80	400	900	440000	
	80-1000	450	1500	57500	
	1000-10000	550		6700	
$\nu_\tau + \bar{\nu}_\tau$	1-4	250	500	1500000	350
	4-10			300000	
	10-50	350	600	375000	
	50-1000	450	800	200000	
	1000-10000	550	1500	26000	

**Table 2.1:** Cylinder volumes used for GENIE neutrino simulation generation. Cylinder is always centered in DeepCore at  $(x, y, z) = (46.29, -34.88, -330.00)$  m.

### 2.1.2 Muons

Atmospheric muons are generated on a cylinder surface enclosing the full IceCube detector array. The cylinder has a height of 1600 m and a radius of 800 m. The energy is sampled from an  $E^{-3}$  power law while the other sampling distributions (position, direction) are found from parameterizations based on [23]. This work uses full CORSIKA [24] simulations of muons to tailor the parameterizations, starting from cosmic ray interactions with atmospheric nuclei using the cosmic ray flux model from [25] and producing the muons applying the hadronic interaction model SIBYLL 2.1 [26]. After the generation, they are propagated through the ice with PROPOSAL producing photons, treating them exactly like the muons produced in neutrino interactions.

Since the offline processing and selection steps described in Section ?? and Section 2.4 reduce the muon contamination to a negligible level, it is difficult to correctly estimate the expected number of muon events at final selection level and therefore two separate sets of muon simulation are produced. A **first set** including all events resulting from the above described generation to tune the lower level selection (up to L4) and a **second set** to estimate the muon contamination at higher levels (above L5), which only accepts muon events if they pass through a smaller cylinder centered in DeepCore (height of 400 m and radius of 180 m) and rejects events based on a KDE estimated muon density at L5 (in energy and zenith) increasing the simulation efficiency at L5 significantly .

[23]: Becherini et al. (2006), "A parameterisation of single and multiple muons in the deep water or ice"

[24]: Heck et al. (1998), "CORSIKA: A Monte Carlo code to simulate extensive air showers"

[25]: Gaisser (2012), "Spectrum of cosmic-ray nucleons, kaon production, and the atmospheric muon charge ratio"

[26]: Engel et al. (2017), "The hadronic interaction model Sibyll – past, present and future"

put a number on this significant increase?

## 2.2 Detector Simulation

The detector simulation is performed after the event generation, where the initial particles and the resulting photons and secondary particles from their propagation were produced. This part of the simulation chain is applied to all particle simulation, both neutrino and muon generation explained in Chapter 2.1, but also the particles from the HNL signal

generation explained in detail in Chapter ?? The detector simulation can be split into two parts, the propagation of the photons and the simulation of the detector response (including internal noise).

### 2.2.1 Photon Propagation

For any Cherenkov detector, but especially for ice-Cherenkov detectors, like IceCube, the propagation of the photons is a crucial part of the detector simulation. Any photon that was produced in the event generation is individually traced through the ice, simulating scattering and absorption processes, taking into account the local ice properties, estimated with a chosen ice model. The propagation is done using CLSIM [27] which is an implementation of the *Photon Propagation Code (PPC)* [28] in OPENCL. It is optimized to be run very efficiently on GPUs, which is what is done for IceCube simulation production. The ice is modeled as a set of 10 m thick, almost horizontal layers with specific absorption and scattering lengths. The *South Pole ICE (SPICE)* model [29] accounts for the layers being tilted by a small amount () and the absorption and scattering lengths having a non-uniformity with respect to the azimuth direction. Figure ?? shows the values of this model for the different depths, indicating the location of IceCube, DeepCore, and the dust layer.

[28]: Chirkin et al. (2019), "Photon Propagation using GPUs by the IceCube Neutrino Observatory"

[29]: Aartsen et al. (2013), "Measurement of South Pole ice transparency with the IceCube LED calibration system"

put a number on the tilt angle?

add plot with ice scattering/absorption lengths used for simulation

[30]: Mie (1908), "Beiträge zur Optik trüber Medien, speziell kolloidaler Metallösungen"

[31]: Henyey et al. (1941), "Diffuse radiation in the Galaxy."

1: When it traveled its full absorption length, sampled in the initial step

In an initial step, each photon's absorption length is sampled from an exponential distribution with the expectation value at the current layer's absorption length. The following propagation steps are performed in parallel for all photons. In each of those steps, corresponding to a single scattering event, the photon travels a length that is sampled from an exponential distribution with the expectation value at the scattering length of the current layer and the scattering angle chosen based on a combination of a simplified Mie scattering distribution [30] and a Henyey-Greenstein distribution [31]. The parameters defining the shape of these distributions were calibrated using data from *in-situ* LED calibration runs. These steps are continuously repeated until each photon reached a DOM or was absorbed <sup>1</sup>. After all photons have been propagated in that manner, the final step is to output the photons that reached a DOM for further processing.

### 2.2.2 Detector Responses

The second part of simulating the IceCube detector is the DOM response itself, but not all the photons that reached a DOM are accepted as being observed. Whether a photon was detected is determined individually based on the total efficiency and the angular acceptance curve of the specific DOM. The total efficiency includes effects of the DOM glass, PMT quantum and photo-electron collection efficiencies, and it is wavelength dependent. Additionally, there is another angle dependent effect called *hole ice*. This effect is due to varied ice properties resulting from the re-freezing process of the water column inside the borehole after deployment of the string. Due to bubble formation the ice is less transparent than the surrounding ice and an additional angular acceptance is added, which can increase or decrease the efficiency to detect photons. Accepted photons are converted into a so-called *Monte Carlo photo-electron (MCPE)*. The amount



of charge measured for each MCPE is determined by sampling from a mixture of two exponential distributions and a normal distribution. This *single photo-electron (SPE)* distribution was tuned to match the observed distribution in each DOM in an *in-situ* calibration study [32]. Figure ?? shows the distribution compared to a lab measurement. Based on the sampled charges and times of MCPEs, the voltage waveforms for the (two) different readout channels are simulated and passed on to the trigger simulation starting with *WaveDeform*, which was already mentioned in Section 1.1.1.

Next to the Cherenkov photons, IceCube also observes photons that are produced in radioactive decays inside the DOMs, both in the glass housing sphere and the PMT glass itself. To simulate this internal noise, the *Vuvuzela* module [33, 34] is used to create additional MCPEs that are fed into the same simulation chain described above. This module takes into account thermal and non-thermal components and their times are sampled using parameterizations of the measured distributions, where the thermal noise component is uncorrelated photons and the non-thermal component is from burst of photons. The noise hits are simulated by drawing the times from a constant rate Poisson process and the number of photons from a Poisson distribution, then the time differences between the individual photons per hit is found, based on a Log-Normal distribution. The simulation is defined by 5 parameters that are calibrated for each DOM individually. Table ?? shows a set of typical values for these parameters.

[32]: Aartsen et al. (2020), “In-situ calibration of the single-photoelectron charge response of the IceCube photomultiplier tubes”

[33]: Larson (2013), “Simulation and Identification of Non-Poissonian Noise Triggers in the IceCube Neutrino Detector”

[34]: Larson (2018), “A Search for Tau Neutrino Appearance with IceCube-DeepCore”

add table with typical vuvuzela noise parameters

## 2.3 Processing

After the detector simulation is performed, all MC and data are processed in exactly the same way. This section explains the trigger and event selection that is applied starting from the raw voltage measured by the PMTs. Most parts of this processing are identical to the procedure already described in [35, 36]. It is split in different steps run inside the ice, at the South Pole, and after the data was transferred to the North. The complexity and computational cost of the processing increases with each step, while the total number of events reduces, making it feasible and reducing the use of computational resources on events that are not of interest for the analysis.

[35]: Trettin (2023), “Search for eV-scale sterile neutrinos with IceCube DeepCore”

[36]: Lohfink (2023), “Testing nonstandard neutrino interaction parameters with IceCube-DeepCore”

### 2.3.1 Trigger and Filter

Before the data can be sent to the North, the initial signal coming from the PMT (for data) or from the detector response simulation (for MC) is a voltage waveform, which has to be digitized and information of photon hits has to be extracted. The trigger and filter explained here are tailored to select events that passed through the DeepCore volume, while rejecting background events (either from atmospheric muons or from random noise). There are other filters used in IceCube which will not be explained here, since they are not relevant for this work. A full description of the instrumentation and the online systems can be found in [37].

[37]: Aartsen et al. (2017), “The IceCube Neutrino Observatory: Instrumentation and Online Systems”

## In-ice Trigger

[4]: Abbasi et al. (2009), “The IceCube data acquisition system: Signal capture, digitization, and timestamping”

[4]: Abbasi et al. (2009), “The IceCube data acquisition system: Signal capture, digitization, and timestamping”

[4]: Abbasi et al. (2009), “The IceCube data acquisition system: Signal capture, digitization, and timestamping”

[1]: Aartsen et al. (2017), “The IceCube Neutrino Observatory: instrumentation and online systems”

[7]: Abbasi et al. (2012), “The design and performance of IceCube DeepCore”

add figure with trigger efficiencies (SMT 3,4,6,8)

2: Where *online* means running on hardware at the South Pole.

The trigger is applied inside the DOM in the ice before sending the information to the ICL on the surface. The time dependent voltage curves are captured if a pre-defined threshold value is exceeded. Once the threshold set to the equivalent of 0.25 PE is crossed, 6.4  $\mu\text{s}$  of the waveform are coarsely digitized by a *Fast Analog-to-Digital Converter (FADC)* with a sampling rate of 40 MHz [4]. Additionally, the first 427 ns are digitized using an *Analog Transient Waveform Recorder (ATWD)* with a sampling rate of 300 MHz [4], but only if some trigger condition is met, because this readout frequency is too high to be sampled directly and requires some buffering. For DeepCore, the HLC condition already mentioned in Section 1.1.1 has to be met for three DOMs inside the fiducial volume within a time window of 5  $\mu\text{s}$ . If this is the case, all waveforms that crossed the threshold within a 20  $\mu\text{s}$  time window around the trigger are digitized and sent to the ICL for further processing. This trigger is called *Simple Multiplicity Trigger 3 (SMT-3)*. The DOM hits that are read out in this process, but do not meet the HLC condition, are called *soft local coincidence (SLC)* hits [4]. The rate of the DeepCore SMT-3 trigger is  $\sim 250$  Hz [1], accepting  $\sim 70\%$  of  $\nu_\mu$ -CC events at 10 GeV and  $\sim 90\%$  at 100 GeV [7]. The trigger efficiencies for different SMT triggers, including the DeepCore SMT-3, are shown in Figure ??.

## Online Filter

The digitized waveforms are sent to the ICL, where a further filter is applied *online*<sup>2</sup>. First the WaveDeform algorithm is run to extract photon arrival times and charge from the waveforms, then the DeepCore filter is applied, which is an iterative hit cleaning starting from HLC hits and removing any hits outside a 125 m radius and a 500 ns time window (called *radius-time cleaning (RT-cleaning)*) of the initial hit. This mainly rejects unphysical SLC hits, which are potentially caused by random noise. The following selection steps are done using the resulting cleaned pulses.

Next, an additional cut is applied to reject events that are likely to be caused by atmospheric muons. This is done by splitting the hits depending on whether they were inside the DeepCore fiducial volume or outside and then calculating the speed of each hit outside the fiducial volume towards the *center of gravity COG* of the hits inside. If one of them has a speed close to the speed of light, the whole event is rejected, because this is a strong indication for a muon event.

As input for the further selection levels, a few event properties, like vertex position and direction, are determined using fast and simple event reconstructions. After the DeepCore online filter, the rate is about 15 Hz, which can be sent to the North via satellite for further processing.

### 2.3.2 Event Selection

After the data was sent to the North, the *offline* filters and selection are applied to further reduce the background of atmospheric muons and noise. The selection is split into three levels referred to as *Level 3-5*

(L3-L5), which bring down the neutrino and muon rate to  $\sim 1$  mHz, while the remaining fraction of random noise is below 1 %.

### Level 3

At the first offline filtering level, Level 3, 1D cuts are used to reduce atmospheric muons, pure noise, and coincident muons. These cuts are targeting regions where the data/MC agreement is poor, so that more sophisticated *machine learning* (ML) techniques can be applied at later levels. The cuts are made using 12 control variables, that are inexpensive to compute for the very large sample at this stage. The variables are related to position, time, and overall number of hits in the event.

Pure noise hits, that are temporally uncorrelated, are cleaned by applying a 300 ns sliding window, requiring the containment of more than 2 hits at its maximum. Additionally, an algorithm is run to check whether the hits show some directionality, accepting them only if they do.

To reduce the amount of muons a series of cuts is applied using spatial and temporal information. Events that have more than 9 hits observed above  $-200$  m or the first HLC hit above  $-120$  m are rejected as well as events where the fraction of hits in the first 600 ns of the event is above 0.37, ignoring the first two hit DOMs. Additionally, the ratio between hits in the veto region and the DeepCore fiducial volume is required to be below 1.5.

If a muon enters the detector after the data acquisition was already triggered, it causes events that span over a much larger time range. To reduce those coincident events, the time difference between first and last pulse cannot be above 5000 ns. This cut mainly affects a region of very poor data to MC agreement, because coincident events are not simulated at all.

The L3 cuts remove 95 % of the atmospheric muons and  $>99$  % of pure noise hits, while keeping  $>60$  % of the neutrino events. The sample now roughly contains muons/neutrinos/noise at a ratio of 100:10:1 with a total rate of  $\sim 0.5$  Hz.

add example plots (??) for L3 cut variables and applied cuts

### Level 4

After the total rate was reduced by the simple cuts of L3 and the overall agreement between data and MC is established, ML techniques can be applied to further reduce the background. For Level 4, two *Boosted Decision Trees* (BDTs) classifier are trained to separate neutrino events from atmospheric muons and noise hits, separately. The output of each classifier, a probability score, can be seen in Figure ?? . The noise filter is applied first and an event passes the score is larger than 0.7, reducing the noise hits by a factor of 100, while keeping 96 % of neutrinos. Then the second BDT classifier, trained partly on unfiltered data consisting of  $>99$  % atmospheric muons, is applied. Rejecting events with a score smaller than 0.65 removes 94 % of atmospheric muons while keeping 87 % of neutrinos. This fraction varies depending on the flavor and interaction type,  $\nu_\mu$ -CC events for example, which have a muon in the final state, are therefore reduced to 82.5 %. After applying the L4 cuts based on the BDT

reference BDT

add figure with L4 BDT classifier outputs

classifier outputs, the sample is still dominated by atmospheric muons, while the noise rate dropped to below most neutrino types.

### Level 5

add some figure showing the corridors?

Level 5 is the final selection level, before event reconstructions are applied. This level aims to reduce the remaining atmospheric muon rate below the rate of neutrinos. Muons not rejected by the earlier levels are those that produced little or no light in the veto regions. One possible reason is that they passed through one of the un-instrumented regions between the strings called *corridors*. To reject those, special corridor cuts, based on the number of hits they produced close to a potential corridor they passed through. The potential corridor in questions is identified based on a simple infinite track fit. In addition to the corridor cuts, starting containment cuts are applied to reject events that start at the edge of the fiducial volume. Events with more than seven hits in the outermost strings of the detector or those that have a down going direction in the uppermost region are rejected. This further reduces the fraction of muons by 96 % while keeping 48 % of neutrinos. The rates after this level are 1 mHz and 2 mHz for neutrinos and muons, respectively, making it a neutrino dominated sample.

add table with rater per level (split in flavor for signal (benchmark mass/mixing?) and background)

## 2.4 Reconstruction

Several methods exist to reconstruct events at the energies relevant for this work (10 GeV to 100 GeV). At these energies, the light deposition is very low and only a few DOMs detect light, making the reconstructions difficult. [38] describes two classical methods, which have partly been applied in one recent IceCube atmospheric neutrino oscillation measurement using a golden<sup>3</sup> sub-sample of the DeepCore sample [19]. The algorithm used in this work on the other hand, is a newer method that applies a *convolutional neural network (CNN)* to reconstruct the events and determine some discriminating quantities. The latest muon neutrino disappearance result from IceCube [39] is based on this reconstruction.

[38]: Abbasi et al. (2022), “Low energy event reconstruction in IceCube DeepCore”

3: add description of what makes this a golden sample

[19]: Abbasi et al. (2023), “Measurement of atmospheric neutrino mixing with improved IceCube DeepCore calibration and data processing”

[39]: Yu et al. (2023), “Recent neutrino oscillation result with the IceCube experiment”

### 2.4.1 Fast Low Energy Reconstruction using Convolutional Neural Networks

As the name *Fast Low Energy Reconstruction using Convolutional Neural Networks (FLERCNN)* already indicates, the FLERCNN reconstruction [40, 41] is a CNN optimized to reconstruct IceCube events at low energies (<100 GeV) in a fast and efficient manner. The network is trained to find the connection between the hit pattern and the events properties by identifying patterns similar to how CNNs are applied effectively in image classification. The patterns are an imprint of the neutrino interactions that can happen anywhere in the detector, which should result in translational invariance of the events. CNNs were shown to have very good performance in identifying patterns in images, independent of their location. By combining several layers of filters of different dimensions, a map of spatial features is created from the input data and more complex

[40]: Yu et al. (2021), “Direction reconstruction using a CNN for GeV-scale neutrinos in IceCube”

[41]: Micallef (),

features can be reconstructed. The architecture of the network is very similar to the preexisting IceCube CNN event reconstruction [42], but optimized on low energy events and specifically tailored to include the DeepCore sub-array. Only the eight DeepCore strings and the central 19 IceCube strings are used for the reconstruction (compare to Figure 1.4). Because of the different z-positions of the DeepCore and IceCube DOMs, they are divided into two networks that are combined at the end (shown in Figure ??). The first dimension of the network is the string index, while the second dimension is the order of the DOMs along the vertical axis. The horizontal position of the DOMs is not used, since the strings are arranged in an irregular pattern. The information from the DOM hits is summarized into five charge and time variables, which make up the last dimension of the input layer. The variables are the total summed charge, the time of the first hit, the charge weighted mean time of the hits, the time of the last hit, and the charge weighted standard deviation of the hit times.

Five different networks are trained using this architecture. Three networks do the regression of the events' energy, zenith angle, and the starting vertex ( $x, y, z$  position), while two of them are used for classification. One to predict the probability of the event being a track (used as PID) and the other to predict the probability of the event being a muon. Each network is trained with a modified training sample, optimized for the task it is performing, but unbiased for the training variable and ideally extending outside the target reconstruction region. Additionally, the activation function and the loss function are adapted, according to the wanted output of the network. For the classification tasks the loss function is the *binary cross entropy* and the activation function is a *sigmoid*. To perform the regression of zenith and vertex position, the loss function is the *mean squared error (MSE)*, while for the energy it is the *mean absolute percentage error*. The activation for all regression tasks is *linear*.

### 2.4.2 Analysis Selection

Before the reconstruction is applied a few additional high level variables are computed, which are from fast and inexpensive algorithms. Then the reconstruction is applied by applying the trained FLERCNN networks to get the output quantities. After that, another BDT classifier is trained to further reduce the muon background for the final sample. The BDT is trained on five high level variables, where three are FLERCNN reconstruction variables (vertex  $z$ ,  $\rho_{36}$ , and muon probability) and two are lower level variables (L4 muon classifier output and L5 corridor cut variable). To train the BDT, the FLERCNN nominal simulation set is used, only using events with  $\cos(\theta_{zenith}) \leq 0.3$ . The output of the BDT is the neutrino probability and a cut at 0.8 is applied to reject events with a high probability of being a muon.

To get the final, pure sample of well reconstructed neutrinos another set of cuts is applied. The first cuts are meant to reject events with poor reconstruction quality, by requiring the events to fall into the DeepCore volume, where the denser, better instrumented detector leads to better resolution. The cuts are applied on the reconstructed radius (distance to string 36 in the center) and z-position of the starting vertex and are listed in Table ?. Additionally rejecting events with fewer than seven

[42]: Huennefeld (2017), "Deep Learning in Physics exemplified by the Reconstruction of Muon-Neutrino Events in IceCube"

add image with selected strings used for flernn IC and DC

add FLERCNN architecture image?

add some performance plots of the FLERCNN reconstruction

There is more information on pre-processing the samples and preparing the input features, and training each cnn, but I'm not sure if that might be too much detail?

hits in the selected DOMs used for the FLERCNN reconstruction showed to increase the resolution. The FLERCNN reconstruction was optimized for atmospheric neutrino analyses which are mainly in the region below 100 GeV. On top of that, there are very few events with energies below 5 GeV, so the reconstructed energy is required to be in that range.

Another set of cuts is applied to make sure the agreement between data and MC is good. To remove coincident muon and neutrino events, cuts are applied to the number of hits in the top 15 layers of IceCube DOMs and the number of hits in the outermost IceCube strings. Coincident random noise events are removed by requiring more than three hit DOMs from direct photons<sup>4</sup>. Neither of the two coincident event types are simulated, which can be seen as bad agreement between data and MC. The last cut is on the reconstructed cosine zenith, which is required to be smaller than 0.04 to reject down-going muons.

4: *Direct photons* are photons that were not scattered on their way from the interaction vertex to the DOM.

add table with final analysis cuts

there is some more information in Elisas thesis about the final sample composition

at some place I will want a selection efficiency for SM BG and HNL signal, but I'm not sure where to put it yet

## 2.5 Systematic Uncertainties

### Neutrino Cross-Section Systematic Uncertainties

- three cross-section uncertainties are included, two for uncertainties in form factors of charged-current quasi-elastic (CCQE) and charged-current resonance (CCRES) events and for uncertainties in deep inelastic scattering (DIS) events

- the uncertainties in the form factors are due to uncertainties in the *axial mass*  $M_A$  which enters the form factor as in

which experiments measure the axial mass?

$$F(Q^2) \sim \frac{1}{(1 - (\frac{Q}{M_A})^2)^2}, \quad (2.2)$$

where  $Q^2$  is the momentum transfer squared

- the axial mass can be determined experimentally and to include uncertainties on the values of  $M_A^{CCQE}$  and  $M_A^{CCRES}$ , the cross-sections are computed with GENIE where the form factors are calculated varying the axial mass by  $\pm 20\%(1\sigma)/\pm 40\%(1\sigma)$  around the nominal value - this is an approximation of the recommended uncertainties by the GENIE collaboration, which are  $-15\%$ ,  $+25\%$  for  $M_A^{CCQE}$  and  $\pm 20\%$  for  $M_A^{CCRES}$  [21] - to apply a continuous uncertainty variation of the axial mass in a fit, the total cross-section is fit with a quadratic function to interpolate between the cross-sections computed with the different axial masses

add varied total cross-section for a few background HNL events

add final level effects of varying the axial mass parameters (or example of one)

[43]: Cooper-Sarkar et al. (2011), "The high energy neutrino cross-section in the Standard Model and its uncertainty"

add DIS systematic effect on final level histograms

- the uncertainty parameter of the DIS cross-section is based on the discrepancy between the cross-sections computed with GENIE and the ones computed with CSMS [43] above 100 GeV - the included parameter scales the cross-section from the GENIE values to the CSMS values, which are considered more accurate above 100 GeV - below 100 GeV the scaling is extrapolated linearly



### 2.5.1 Atmospheric Flux

### 2.5.2 Detector Property Variations

#### Muon Uncertainties

- final level muon fraction is below a percent - just include a total scaling parameter in the analysis (- total scale is degenerate with DOM efficiency, since increased DOM efficiency approximately leads to better muon rejection) - changes in the muon spectral index have a negligible effect on the final level histograms and the analysis (see systematic impact test in section xx)

add muon systematic effects  
(total scale and ) on final  
level histograms





# Bibliography

Here are the references in citation order.

- [1] M. G. Aartsen et al. “The IceCube Neutrino Observatory: instrumentation and online systems”. In: *Journal of Instrumentation* 12.3 (Mar. 2017), P03012. doi: [10.1088/1748-0221/12/03/P03012](https://doi.org/10.1088/1748-0221/12/03/P03012) (cited on pages 1, 3, 16).
- [2] P. B. Price, K. Woschnagg, and D. Chirkin. “Age vs depth of glacial ice at South Pole”. In: *Geophysical Research Letters* 27.14 (2000), pp. 2129–2132. doi: <https://doi.org/10.1029/2000GL011351> (cited on page 2).
- [3] R. Abbasi et al. “In-situ estimation of ice crystal properties at the South Pole using LED calibration data from the IceCube Neutrino Observatory”. In: *The Cryosphere Discussions* 2022 (2022), pp. 1–48. doi: [10.5194/tc-2022-174](https://doi.org/10.5194/tc-2022-174) (cited on page 2).
- [4] R. Abbasi et al. “The IceCube data acquisition system: Signal capture, digitization, and timestamping”. In: *Nuclear Instruments and Methods in Physics Research Section A: Accelerators, Spectrometers, Detectors and Associated Equipment* 601.3 (2009), pp. 294–316. doi: <https://doi.org/10.1016/j.nima.2009.01.001> (cited on pages 2, 3, 16).
- [5] M. G. Aartsen et al. “Energy Reconstruction Methods in the IceCube Neutrino Telescope”. In: *JINST* 9 (2014), P03009. doi: [10.1088/1748-0221/9/03/P03009](https://doi.org/10.1088/1748-0221/9/03/P03009) (cited on page 3).
- [6] N. Kulacz. “In Situ Measurement of the IceCube DOM Efficiency Factor Using Atmospheric Minimum Ionizing Muons”. MA thesis. University of Alberta, 2019 (cited on page 3).
- [7] R. Abbasi et al. “The design and performance of IceCube DeepCore”. In: *Astropart. Phys.* 35.10 (2012), pp. 615–624. doi: [10.1016/j.astropartphys.2012.01.004](https://doi.org/10.1016/j.astropartphys.2012.01.004) (cited on pages 3, 16).
- [8] P. A. Cherenkov. “Visible Radiation Produced by Electrons Moving in a Medium with Velocities Exceeding that of Light”. In: *Phys. Rev.* 52 (4 Aug. 1937), pp. 378–379. doi: [10.1103/PhysRev.52.378](https://doi.org/10.1103/PhysRev.52.378) (cited on page 4).
- [9] S. Euler. “Observation of oscillations of atmospheric neutrinos with the IceCube Neutrino Observatory”. PhD thesis. Aachen, Germany: Rheinisch-Westfälischen Technischen Hochschule, 2014 (cited on page 5).
- [10] I. Frank and I. Tamm. “Coherent visible radiation from fast electrons passing through matter”. In: *C. R. Acad. Sci. USSR* 14 (1937), pp. 109–114 (cited on page 5).
- [11] I. Tamm. “Radiation Emitted by Uniformly Moving Electrons”. In: *Selected Papers*. Ed. by B. M. Bolotovskii, V. Y. Frenkel, and R. Peierls. Berlin, Heidelberg: Springer Berlin Heidelberg, 1991, pp. 37–53. doi: [10.1007/978-3-642-74626-0\\_3](https://doi.org/10.1007/978-3-642-74626-0_3) (cited on page 5).
- [12] L. Rädcl and C. Wiebusch. “Calculation of the Cherenkov light yield from low energetic secondary particles accompanying high-energy muons in ice and water with Geant4 simulations”. In: *Astroparticle Physics* 38 (Oct. 2012), pp. 53–67. doi: [10.1016/j.astropartphys.2012.09.008](https://doi.org/10.1016/j.astropartphys.2012.09.008) (cited on pages 5, 12).
- [13] D. Chirkin and W. Rhode. “Propagating leptons through matter with Muon Monte Carlo (MMC)”. In: (July 2004) (cited on page 6).
- [14] L. Raedel. “Simulation Studies of the Cherenkov Light Yield from Relativistic Particles in High-Energy Neutrino Telescopes with Geant4”. MA thesis. Aachen, Germany: Rheinisch-Westfälischen Technischen Hochschule, 2012 (cited on pages 6, 7).
- [15] M. Tanabashi et al. “Review of Particle Physics”. In: *Phys. Rev. D* 98 (3 Aug. 2018), p. 030001. doi: [10.1103/PhysRevD.98.030001](https://doi.org/10.1103/PhysRevD.98.030001) (cited on page 6).
- [16] S. Agostinelli et al. “Geant4—a simulation toolkit”. In: *Nucl. Instr. Meth. Phys. Res.* 506.3 (July 2003), pp. 250–303. doi: [10.1016/S0168-9002\(03\)01368-8](https://doi.org/10.1016/S0168-9002(03)01368-8) (cited on pages 6, 12).

- [17] T. Gabriel et al. “Energy dependence of hadronic activity”. In: *Nuclear Instruments and Methods in Physics Research Section A: Accelerators, Spectrometers, Detectors and Associated Equipment* 338.2 (1994), pp. 336–347. doi: [https://doi.org/10.1016/0168-9002\(94\)91317-X](https://doi.org/10.1016/0168-9002(94)91317-X) (cited on page 7).
- [18] A. Terliuk. “Measurement of atmospheric neutrino oscillations and search for sterile neutrino mixing with IceCube DeepCore”. PhD thesis. Berlin, Germany: Humboldt-Universität zu Berlin, Mathematisch-Naturwissenschaftliche Fakultät, 2018. doi: [10.18452/19304](https://doi.org/10.18452/19304) (cited on page 8).
- [19] R. Abbasi et al. “Measurement of atmospheric neutrino mixing with improved IceCube DeepCore calibration and data processing”. In: *Phys. Rev. D* 108 (1 July 2023), p. 012014. doi: [10.1103/PhysRevD.108.012014](https://doi.org/10.1103/PhysRevD.108.012014) (cited on pages 11, 18).
- [20] M. Honda et al. “Atmospheric neutrino flux calculation using the NRLMSISE-00 atmospheric model”. In: *Phys. Rev. D* 92 (2 July 2015), p. 023004. doi: [10.1103/PhysRevD.92.023004](https://doi.org/10.1103/PhysRevD.92.023004) (cited on page 12).
- [21] C. Andreopoulos et al. “The GENIE Neutrino Monte Carlo Generator: Physics and User Manual”. In: (2015) (cited on pages 12, 20).
- [22] J.-H. Koehne et al. “PROPOSAL: A tool for propagation of charged leptons”. In: *Computer Physics Communications* 184.9 (2013), pp. 2070–2090. doi: <https://doi.org/10.1016/j.cpc.2013.04.001> (cited on page 12).
- [23] Y. Becherini et al. “A parameterisation of single and multiple muons in the deep water or ice”. In: *Astroparticle Physics* 25.1 (2006), pp. 1–13. doi: <https://doi.org/10.1016/j.astropartphys.2005.10.005> (cited on page 13).
- [24] D. Heck et al. “CORSIKA: A Monte Carlo code to simulate extensive air showers”. In: (Feb. 1998) (cited on page 13).
- [25] T. K. Gaisser. “Spectrum of cosmic-ray nucleons, kaon production, and the atmospheric muon charge ratio”. In: *Astropart. Phys.* 35 (2012), pp. 801–806. doi: [10.1016/j.astropartphys.2012.02.010](https://doi.org/10.1016/j.astropartphys.2012.02.010) (cited on page 13).
- [26] R. Engel et al. “The hadronic interaction model Sibyll – past, present and future”. In: *EPJ Web Conf.* 145 (2017). Ed. by B. Pattison, p. 08001. doi: [10.1051/epjconf/201614508001](https://doi.org/10.1051/epjconf/201614508001) (cited on page 13).
- [27] C. Kopper et al. <https://github.com/claudiok/clsim> (cited on page 14).
- [28] D. Chirkin et al. “Photon Propagation using GPUs by the IceCube Neutrino Observatory”. In: *2019 15th International Conference on eScience (eScience)*. 2019, pp. 388–393. doi: [10.1109/eScience.2019.00050](https://doi.org/10.1109/eScience.2019.00050) (cited on page 14).
- [29] M. G. Aartsen et al. “Measurement of South Pole ice transparency with the IceCube LED calibration system”. In: *Nucl. Instrum. Meth. A* 711 (2013), pp. 73–89. doi: [10.1016/j.nima.2013.01.054](https://doi.org/10.1016/j.nima.2013.01.054) (cited on page 14).
- [30] G. Mie. “Beiträge zur Optik trüber Medien, speziell kolloidaler Metallösungen”. In: *Annalen der Physik* 330.3 (1908), pp. 377–445. doi: <https://doi.org/10.1002/andp.19083300302> (cited on page 14).
- [31] L. G. Henyey and J. L. Greenstein. “Diffuse radiation in the Galaxy.” In: *apj* 93 (Jan. 1941), pp. 70–83. doi: [10.1086/144246](https://doi.org/10.1086/144246) (cited on page 14).
- [32] M. G. Aartsen et al. “In-situ calibration of the single-photoelectron charge response of the IceCube photomultiplier tubes”. In: *Journal of Instrumentation* 15.6 (June 2020), P06032. doi: [10.1088/1748-0221/15/06/P06032](https://doi.org/10.1088/1748-0221/15/06/P06032) (cited on page 15).
- [33] M. Larson. “Simulation and Identification of Non-Poissonian Noise Triggers in the IceCube Neutrino Detector”. Available at <https://ir.ua.edu/handle/123456789/1927>. MA thesis. University of Alabama, Tuscaloosa, AL, USA, 2013 (cited on page 15).
- [34] M. Larson. “A Search for Tau Neutrino Appearance with IceCube-DeepCore”. available at [https://discoverycenter.nbi.ku.dk/teaching/thesis\\_page/mjlarsen\\_thesis.pdf](https://discoverycenter.nbi.ku.dk/teaching/thesis_page/mjlarsen_thesis.pdf). PhD thesis. University of Copenhagen, Denmark, 2018 (cited on page 15).
- [35] A. Trettin. “Search for eV-scale sterile neutrinos with IceCube DeepCore”. PhD thesis. Berlin, Germany: Humboldt-Universität zu Berlin, Mathematisch-Naturwissenschaftliche Fakultät, 2023. doi: <https://github.com/atrettin/PhD-Thesis> (cited on page 15).

- [36] E. Lohfink. “Testing nonstandard neutrino interaction parameters with IceCube-DeepCore”. PhD thesis. Mainz, Germany: Johannes Gutenberg-Universität Mainz, Fachbereich für Physik, Mathematik und Informatik, 2023. doi: <http://doi.org/10.25358/openscience-9288> (cited on page 15).
- [37] M. G. Aartsen et al. “The IceCube Neutrino Observatory: Instrumentation and Online Systems”. In: *JINST* 12.03 (2017), P03012. doi: [10.1088/1748-0221/12/03/P03012](https://doi.org/10.1088/1748-0221/12/03/P03012) (cited on page 15).
- [38] R. Abbasi et al. “Low energy event reconstruction in IceCube DeepCore”. In: *Eur. Phys. J. C* 82.9 (2022), p. 807. doi: [10.1140/epjc/s10052-022-10721-2](https://doi.org/10.1140/epjc/s10052-022-10721-2) (cited on page 18).
- [39] S. Yu and J. Micallef. “Recent neutrino oscillation result with the IceCube experiment”. In: *38th International Cosmic Ray Conference*. July 2023 (cited on page 18).
- [40] S. Yu and on behalf of the IceCube collaboration. “Direction reconstruction using a CNN for GeV-scale neutrinos in IceCube”. In: *Journal of Instrumentation* 16.11 (2021), p. C11001. doi: [10.1088/1748-0221/16/11/C11001](https://doi.org/10.1088/1748-0221/16/11/C11001) (cited on page 18).
- [41] J. Micallef. <https://github.com/jessimic/LowEnergyNeuralNetwork> (cited on page 18).
- [42] M. Huennefeld. “Deep Learning in Physics exemplified by the Reconstruction of Muon-Neutrino Events in IceCube”. In: *PoS ICRC2017* (2017), p. 1057. doi: [10.22323/1.301.1057](https://doi.org/10.22323/1.301.1057) (cited on page 19).
- [43] A. Cooper-Sarkar, P. Mertsch, and S. Sarkar. “The high energy neutrino cross-section in the Standard Model and its uncertainty”. In: *JHEP* 08 (2011), p. 042. doi: [10.1007/JHEP08\(2011\)042](https://doi.org/10.1007/JHEP08(2011)042) (cited on page 20).